

## **LIDAR REMOTE SENSING**

Dr. Matthew McGill  
NASA Goddard Space Flight Center  
Laboratory for Atmospheres  
Greenbelt, MD 20771  
phone: 301-614-6281  
fax: 301-614-5492  
email: [mcgill@virl.gsfc.nasa.gov](mailto:mcgill@virl.gsfc.nasa.gov)

Submitted to The Encyclopedia of Optical Engineering  
March, 2002

## INTRODUCTION

The laser radar, or lidar (for *light detection and ranging*) is an important tool for atmospheric studies. Lidar provides a unique and powerful method for unobtrusively profiling aerosols, wind, water vapor, temperature, and other atmospheric parameters. This brief overview of lidar remote sensing is focused on atmospheric applications involving pulsed lasers. The level of technical detail is aimed at the educated non-lidar expert and references are provided for further investigation of specific topics. The article is divided into three main sections. The first describes atmospheric scattering processes and the physics behind laser-atmosphere interactions. The second section highlights some of the primary lidar applications, with brief descriptions of each measurement capability. The third section describes the practical aspects of lidar operation, including the governing equation and operational considerations.

## BACKGROUND

Remote sensing can be generically defined as the act of measuring some aspect of an object without actually being in contact with the object. Although many disciplines use remote sensing techniques, atmospheric science is a discipline with particular need for remote sensing measurements. Early remote sensing techniques such as sounding rockets and balloons have given way to new classes of active and passive remote sensors. The first significant active remote sensing advancement was the development of radar. Introduced during World War II and perfected for scientific uses thereafter, radar has become a primary tool for atmospheric studies. The next advancement came with the development and deployment of weather satellites.

Operation of weather satellites such as GOES, TIROS-N, and DMSP have allowed unprecedented advances in atmospheric science and operational forecasting.(1)

Among the more recent developments in remote sensing is the laser radar, or lidar (which stands for *light detection and ranging*). In essence, lidar is optical radar, operating in the visible and near-visible wavelength regions. The first true lidar measurements were made in 1963 using a pulsed ruby laser.(2) By the mid-1960s it was clearly established that lasers could provide an optimal source of electromagnetic radiation for atmospheric studies.(3)(4) With highly monochromatic and collimated output beams and with discrete pulses of energy lasers quickly became the focus for instrumentation to study the atmospheric state. Since the late 1960s, lidar remote sensing has been used to measure cloud and aerosol properties, wind motions, temperature, major and trace constituent concentrations, and numerous other atmospheric parameters. Other applications, such as profiling of surface topography and measurements of ocean color also rely on the basic concept of lidar remote sensing.

In the most fundamental sense, all lidar systems consist of a transmitter and a receiver. The transmitter invariably includes the laser and a beam expander to set the outgoing beam divergence. If azimuth-elevation scanning is desired the system also has a mirror system to direct the beam to the proper angles. The receiver includes a telescope to collect backscattered signal, appropriate optics to direct the return signal from the telescope to the detector, and a detector(s) to count the signal. Figure 1 shows a high-level view of the generic lidar system.

Specific characteristics of the lidar system are determined by the parameter(s) to be measured. Different atmospheric parameters levy different requirements on the laser. For example, cloud/aerosol measurements can utilize broadband multi-mode lasers, whereas measurements of constituent concentration or wind require narrow linewidth, single longitudinal mode lasers. Similarly, each atmospheric parameter imposes different requirements on the receiver system. Photons backscattered to the receiver contain information on physical and spectral characteristics of the scattering particles. The specific characteristic(s) to be measured determines the specifics, and the complexity, of the receiver. Wind measuring lidars must be capable of resolving Doppler shifts, depolarization lidars require optics for polarization discrimination, and Raman lidars must be able to isolate specific absorption features. Suffice to say that most lidar systems are specific to measuring a certain variable. Designing a system with the flexibility to measure several different variables seems not to be a consideration for most researchers. One notable exception, however, is the Arctic Lidar Observatory for Middle Atmosphere Research (ALOMAR) Rayleigh/Mie/Raman system, which is designed to simultaneously measure density, temperature, winds, and cloud/aerosol properties.(5)

## ATMOSPHERIC SCATTERING PROCESSES

Before discussing details of lidar systems and measurements it is necessary to understand how the atmosphere interacts with radiation. This discussion will provide only a cursory overview, but several excellent references exist that can be consulted for more detail.(6)(7)(8) Laser light propagating into the atmosphere will be transmitted, reflected, or absorbed when it encounters a particle. Which process occurs at any given radiation-particle interface depends on the

wavelength of the incident radiation and the physical characteristics of the particle. Particles in the atmosphere are classified into two groups: molecules and aerosols. Each group has distinctly different physical and scattering characteristics and it is important to understand the basic differences between the two.

Molecular scattering represents the minimum scattering that can occur at any level in the atmosphere. That is, molecules are present even in regions where aerosols are not and thus represent a background scattering. Another characteristic of molecules is their small size, with radii on the order of  $10^{-4}$   $\mu\text{m}$ . Scattering by molecules is termed Rayleigh scattering after Lord Rayleigh who first developed the mathematical description for scattering by small particles. Rayleigh scattering theory applies to particles with radii less than 0.03 times the wavelength of the incident radiation ( $r < 0.03\lambda$ ). Most notably, Rayleigh scattering is characterized by a  $\lambda^{-4}$  dependence. The strong wavelength dependence means that shorter wavelengths are scattered more efficiently than longer wavelengths.

When light is incident on a particle, the particle removes energy from the light wave and re-radiates the energy. The pattern of radiated energy is centered on the particle and is characteristic of the size of the particle relative to the wavelength of the incident light. This should not be surprising, since larger particles present a larger obstacle to the light wave. The radiated (or “scattered”) energy is not necessarily distributed uniformly, as illustrated in Figure 2, which shows scattered energy patterns (called phase functions) as a function of angle for different relative particle sizes. Molecular scattering is characterized by equal amounts of energy scattered in the forward and backward directions, as shown in Figure 2(a). One further way to differentiate

molecular and aerosol scattering is by the scattering cross-section. The scattering cross-section describes how large an obstruction a particle presents to an incident light wave and is related to the integral area of the phase function. Typical Rayleigh scattering cross-sections at visible wavelengths are on the order of  $10^{-27} \text{ cm}^2$ .(9)

A final difference between aerosol and Rayleigh scattering is the spectral width of the scattered light. Light scattered from both aerosols and molecules will be spectrally broadened (Doppler-broadened) due to random thermal motions. Aerosol scattering has only a small broadening effect, characterized by a Lorentzian form, because the relatively massive aerosol particles have little thermal velocity.(10)(11) Molecules, however, are lighter and have greater thermal velocity, leading to considerable spectral broadening. Typical Rayleigh scattering widths in the visible region are on the order of 2 GHz, and the spectral shape is characterized by a Gaussian function.(10) The difference in spectral widths is illustrated in Figure 3.

As the particle radius increases beyond  $\sim 0.03\lambda$ , Rayleigh theory breaks down. Mie theory was developed to describe scattering by larger particles, and Mie theory reduces to Rayleigh theory for small particle sizes. Mie scattering theory is necessary to describe scattering by large aerosol particles and is characterized by complicated phase functions, as shown in Figure 2(b,c). As the particle size increases, the scattering pattern becomes increasingly complex and more of the scattered light is concentrated in the forward direction. Also, as the particle size increases, the scattering has less dependence on wavelength. Clouds and fog are composed of large droplets (radii  $\sim 1-10 \mu\text{m}$ ) that scatter light according to Mie theory. This explains why clouds, fog, and haze appear white, since all wavelengths scatter about equally. For comparison with Rayleigh

scattering, typical aerosol scattering cross-sections are on the order of  $10^{-14}$  cm<sup>2</sup>. The distribution of aerosols is not as uniform as that for molecules and there are large regions of the atmosphere with little aerosol content.

In addition to simple elastic scattering, other processes can occur when radiation encounters a particle. Absorption in the atmosphere occurs when the incident radiation is at the same wavelength as an absorption line in a molecular species. Primary absorbing species in the atmosphere are water vapor, carbon dioxide, and ozone. Resonance scattering occurs if the laser wavelength is matched to the wavelength of an atomic or molecular transition. Raman scattering is an inelastic scattering process that can occur if the energy difference between the incident and radiated photon matches a transition between energy levels in a molecule.

Why is all this important? Because designing a lidar system to measure some parameter in the atmosphere requires attention to the physical processes of particle scattering. Note, for example, that aerosol scattering is strongly peaked in the forward direction (Figure 2), whereas lidar systems typically observe the 180-degree backscatter. Will the lidar use aerosol or molecular backscatter, or both, as the signal source? If using aerosol backscatter, how much contamination will occur due to Rayleigh scattering? Is the laser wavelength located in a strong absorption line? All these questions, among many others, drive the fundamental instrument design.

## LIDAR TECHNIQUES FOR ATMOSPHERIC MEASUREMENTS

This section provides an overview of lidar measurement capabilities. This overview is not intended to be all-inclusive, but merely to illustrate some of the demonstrated measurement techniques that have been developed. The references listed are not all inclusive, nor are they meant to provide an historical accounting of the topics. A thorough and historically complete compilation of lidar measurement capabilities can be found in Measures (ref. 8). Selected references are provided to facilitate further investigation of particular topics and are intended to showcase a cross-section of lidar research and researchers. The interested reader will find the references a useful starting point for detailed investigation of specific subjects.

### Aerosol Backscatter Lidar

The least complex lidar is the simple aerosol backscatter system. Such systems are used to determine cloud and aerosol boundaries and structure and also to measure aerosol optical properties, such as optical depth, depolarization, or extinction. Measurements of aerosol properties are, in general, difficult to obtain. Aerosols span a wide range of sizes, from roughly about  $10^{-4}$   $\mu\text{m}$  up to millimeters. The chemical composition of aerosols can be changed by reactions with the measuring device or by evaporation during the measurement process. While optical devices such as nephelometers can avoid degrading the sample, obtaining altitude profiles of particle characteristics is a primary application for lidar.

A considerable body of research exists on lidar studies of cloud and aerosol characteristics. Cirrus clouds, in particular, have long been a target for lidar research.(12)(13)(14)(15) Cirrus and sub-visual cirrus play a key role in radiative transfer in the atmosphere, are less optically dense

than water clouds, and can easily display dynamic features such as wave motions.(16) Because cirrus tend to be optically thin, using radar to study cirrus is problematic because most radar systems lack the sensitivity required to see optically thin layers. Lidars, in contrast, have greater sensitivity to small particles and are well suited to studies of optically thin media. Lidar studies of aerosol type and extinction (17)(18)(19) and depolarization (20)(21)(22)(23) have also been areas of intense research activity. Measurement of the depolarization ratio provides information on the shape of the scattering particle and is useful for determining the phase (ice or water) of clouds.

In addition to vertical profiling capability, spaceborne lidar systems will allow global coverage for monitoring of various parameters such as cloud cover, cloud height, and aerosol distribution. Given that aerosol backscatter systems are the simplest of lidar implementations (having the least demanding requirements for the laser and receiver), it should not be surprising that the first spaceborne lidar systems will be of this type. To date, the only lidar system that has operated from a spaceborne platform was the Lidar In-space Technology Experiment (LITE) onboard the Space Shuttle in 1994.(24) However, two projects are underway that will lead to operational global profiling of clouds and aerosols. The Geoscience Laser Altimeter System (GLAS) on the ICESat satellite is scheduled for launch in 2002-03.(25) The Cloud-Aerosol Lidar and Infrared Pathfinder Satellite Observations (CALIPSO), a dedicated cloud-aerosol profiling lidar mission, is targeted for launch in 2004.(26)

Doppler Lidar

As early as 1972 (11) it was shown that particle motions in the atmosphere accurately represent the mean wind velocity. The Doppler shift imparted to light that elastically scatters from a particle is related to the line-of-sight velocity of that particle, which is assumed to be equal to the mean wind velocity. The challenge for a Doppler lidar system is to resolve the small Doppler shifts inherent to atmospheric motions. For example, if using a 532 nm source, a mean wind of 10 m/s imparts a Doppler shift of only  $3.5 \times 10^{-5}$  nm.

There are two types of wind-measuring lidar: coherent detection and direct detection. Coherent detection is a heterodyning technique that mixes the return signal with a second laser beam, usually a local oscillator offset in frequency.(27)(28)(29) The mixing generates a beat frequency that is related to the Doppler shift. Coherent systems operate by comparing the phase of the backscattered signal with the phase of the reference laser. To maintain phase coherence imposes a limitation on the coherent method: it requires phase coherence across the entire field of view of the receiving optics. This demands diffraction-limited optics and thus limits the maximum size of the receiving telescope.

Both coherent detection and direct detection Doppler lidars require lasers with good frequency stability. Coherent systems operate at longer wavelengths, typically 2  $\mu\text{m}$  or greater because diffraction limited optics are more challenging at shorter wavelengths. Unfortunately, operation at longer wavelengths depends on larger sized particles for effective scattering, which is a limitation considering that the concentration of larger particles drops off rapidly with altitude. Coherent detection works only when aerosol particles of adequate cross-section are present.

However, provided the aerosol scatterers are present, the accuracy of the coherent measurement can be high.(30)

In contrast, direct detection relies on directly sensing the Doppler shift by measuring the wavelength shift of the return signal. The laser wavelength is measured before the atmosphere affects the pulse to determine a zero-wind reference. Subsequent measurements of the atmosphere-scattered light will reveal a wavelength offset that is proportional to the Doppler shift. Fabry-Perot interferometers are usually employed to produce the desired spectral resolution. The direct detection method does not require diffraction-limited optics or phase coherence, so there is no limitation on telescope size. Direct detection Doppler lidars can operate at shorter wavelengths where aerosols are more prevalent. Several lidar groups have successfully used this approach.(11)(31)(32)(33)(34) Direct detection can also use capitalize on the ubiquity of molecular backscatter. Using Rayleigh scattering as the spectral source permits measurements in aerosol-free conditions, although with reduced accuracy due the greater spectral width.(35)(36)(37)

### Raman Lidar

Unlike Mie scattering, Raman scattering is an inelastic scattering process. This means the light is absorbed and re-emitted at a different frequency rather than scattering back at the original frequency. The Raman technique is useful because different chemical species will behave differently when influenced by light of a given frequency. The difference in energy between the absorbed and emitted light will be characteristic of the scattering molecule, and is associated

with a vibrational or rotational energy change. Thus, with proper choice of laser wavelength Raman lidars can measure the relative abundance of certain chemical species. Water vapor content of the atmosphere is a common measurement by Raman lidar.(38)(39) Other parameters that can be measured using Raman lidar include ozone (40) and temperature.(41)(42)

A limitation for Raman lidar is that Raman scattering cross-sections are small, thus limiting the usefulness of this technique to measuring major constituents (water vapor, ozone, nitrogen). Raman scattering has the same  $\lambda^{-4}$  dependence as Rayleigh scattering, but Raman scattering cross-sections are at least two orders of magnitude smaller than Rayleigh scattering cross-sections.(43) Also, because the Raman backscattered signal is so weak, careful consideration must be given to eliminating the elastically-backscattered signal.

### Resonance Scattering Lidar

Resonance scattering is frequently used to study trace constituents in the atmosphere. To effect this lidar method, the laser wavelength is matched to the (known) wavelength of an atomic transition. Thus, light incident on the atom will excite the atom to a higher energy state and the atom will then re-emit at the same wavelength. However, there will be a time delay before the reemission occurs that corresponds to the radiative lifetime of the transition. This is an effective technique in certain areas of the upper atmosphere where the laser light will not be affected by other scatterers. An example is the sodium layer that resides in the 80-105 km altitude range. By matching the laser wavelength to that of a particular transition in the sodium atom, temperature measurements based on thermal broadening of the laser line can be made through that

region.(44) Unlike Raman scattering, resonance scattering cross-sections tend to be rather large. The return signal can still be limited, however, by collisional quenching of the atomic energy.

### High Spectral Resolution Lidar (HSRL)

High spectral resolution lidar (HSRL) has the capability of separating the return signal into aerosol and molecular components. In this way, Rayleigh scattering can be removed, leaving only the aerosol signal and thereby allowing a direct determination of the aerosol extinction and optical properties.(45)(46) The HSRL lidar technique is capable of providing measurements of aerosol properties including: optical depth, extinction cross section, backscatter cross section, and, in certain conditions, backscatter phase function.

To understand the necessity of high resolving capability recall that the spectral signature of Rayleigh scattering is on the order of 2 GHz ( $\sim 10^{-3}$  nm) as shown in Figure 3. The aerosol linewidth, in contrast, is virtually a delta function (on the order of 10 MHz, or  $10^{-5}$  nm). The only way to isolate the aerosol spectral shape is to use a Fabry-Perot interferometer or other narrow filter, such as an iodine absorption cell. A complicating factor for this lidar technique is the laser linewidth. Most pulsed lasers have a finite spectral width that is much greater than the aerosol linewidth, so special attention is required to ensure that the laser spectral width remains small and does not compromise the aerosol-Rayleigh separation. Generally, frequency-stabilized injection-seeded lasers are required to produce a linewidth narrow enough to enable the HSRL measurement.

## Differential Absorption Lidar (DIAL)

Differential Absorption Lidar (DIAL) techniques use two or more wavelengths to measure concentrations of certain chemical species. Typically, one of the laser wavelengths is chosen to correspond to the peak of an absorption line of the chosen chemical species. The second laser wavelength is chosen to be slightly offset from the peak of the absorption line. Both wavelengths are used to probe the same volume of atmosphere, so the ratio of the backscattered intensities is related to the concentration of the chemical species. Water vapor and ozone are two commonly measured atmospheric constituents.<sup>(39)(47)(48)(49)</sup> Pollution monitoring also relies heavily on the DIAL technique for measurements of species such as carbon monoxide, nitrogen dioxide, sulfur dioxide, and other constituents.

DIAL techniques do have a couple of limitations that should be considered. First, the measurement is dependent on accurate knowledge of the absorption coefficient for the particular absorbing gas. Second, since the laser must be accurately tuned to the absorption line, the width of the absorption line must be considered.<sup>(39)</sup> These issues notwithstanding, the DIAL method allows measurement of various chemical profiles from the ground up to about 50 km, rendering it a powerful remote sensing technique.

## Laser Altimetry and Other Measurements

There are many other measurement applications for lidar and lidar-related techniques. A few of those applications will be mentioned here, but this is not intended as an exhaustive compilation.

Topographic profiling, or laser altimetry, is an important application that is similar to standard lidar measurements but uses short laser pulses and electronics with fast sample rates to obtain centimeter-type vertical resolution. Topographic profiling systems have been used for terrain mapping,(50) vegetation canopy mapping,(51) and measurements of ice sheet evolution.(52) The Mars Orbiter Laser Altimeter (MOLA) has provided unprecedented mapping of the Martian surface.(53) Lidar observations of ocean surfaces using a laser fluorescence spectrometer can provide data for use in phytoplankton and ocean color studies.(54)(55) Ocean wave displacement measurements are useful for ocean roughness and motion studies.(56)

## FUNDAMENTALS OF LIDAR

There are two fundamental factors that enable lidar measurements: lasers with discrete pulses and the constancy of the speed of light. Temporal isolation of the light pulse unambiguously determines the region of atmosphere that contributes to the detected signal. Figure 4 schematically illustrates the lidar timing concept. As the laser pulse is emitted and propagates through the atmosphere it is elementary to determine how far the pulse has traveled in a given time. If the altitude resolution (also called range resolution, or range bin length) of the lidar system is  $\Delta r$ , then the range bin length can be written as  $\Delta r = ct/2$ . The factor of 1/2 accounts for the fact that light must make a round trip over the distance  $\Delta r$  and also leads to the old joke that “lidar light only travels half as fast as normal light.” Thus, if the altitude resolution of the system is 150 m then it takes 1  $\mu\text{sec}$  for the laser pulse to cover the round trip distance.

A common misconception about the lidar technique is that signal can only be measured from one range bin per laser pulse. In fact, one of the strengths of lidar remote sensing is that signal can be measured from all range bins (up to the limit of signal attenuation) from each laser pulse. In practice, fast electronics are used to count the detector output signal over the temporal duration of a range bin. At the end of each range bin the electronics reset to begin counting signal from the next range bin. The process of counting and resetting at each successive range bin is referred to as range gating. The range bin length and number of range bins collected can vary according to the parameter being measured, desired vertical resolution of the measurement, and response time of the detector and electronics being used.

By their very nature lidar systems provide measurements over a volume, rather than the point measurements associated with in situ instruments. Lidar measurements are thus more representative of the atmospheric state since spatially averaged measurements minimize the effects of turbulence and localized structure. The volume being averaged can be varied by changing the range bin length (integration time) and the receiver field of view. Scanning telescopes, or use of multiple telescopes, can increase the volume being probed. Also, because the telescope field of view has a given divergence angle, the volume being averaged necessarily increases with distance from the transmitter, as can be seen from Figure 5.

The receiving telescope and the outgoing laser beam can be situated side-by-side (i.e., biaxially) or the laser beam can exit along the same optical axis as the telescope (i.e., coaxially). Figure 6 illustrates the geometry of both approaches. The coaxial arrangement will achieve full overlap of the transmitter and receiver at near range whereas the biaxial arrangement will achieve full

overlap at greater distances. The term overlap refers to the fraction of the transmitted beam cone falling within the receiver field of view and describes the fact the telescope cannot simultaneously be focused at all ranges. Alternately, the overlap function describes the geometric probability that light scattered from a certain range will reach the detector. The range at which full overlap occurs is dependent upon several parameters, including the telescope field of view, laser beam divergence, temporal shape of the laser beam, obscuration due to telescope secondary mirror, and separation of the laser and telescope axes. As shown in Figure 6, it is obvious that in the near field region the overlap will be less than unity. If calibrated measurements are to be obtained in this region then the overlap must be calculated and used to correct the measured signal. It is also obvious from Figure 6 that for best efficiency the laser beam divergence must be smaller than the telescope field of view. A full mathematical treatment of the overlap calculation can be found in Measures (ref. 8).

### The Lidar Equation

A single mathematical expression governs lidar remote sensing. Known as the lidar equation, the expression relates the backscattered signal to the instrumental parameters, optical properties of the atmosphere, and geometrical factors. An excellent derivation of the lidar equation, starting from basic physical principles, can be found in texts by Liou (ref. 7) and Measures (ref. 8). The basic scattering lidar equation describes the number of photons,  $N(r)$ , detected from range  $r$ :

$$N(r) = \left\{ \left[ \left( \frac{E_T \lambda}{hc} \right) \Delta r Q_E T_O O_A(r) \left[ \frac{A_T}{r^2} \right] \left[ (P_A(\pi, r) \beta_A(r) + P_M(\pi, r) \beta_M(r)) e^{-2 \int_0^r \sigma(r') dr'} \right] \right] \right\} + B_D + B_S$$

$$N(r) = \left[ \left( \frac{E_T \lambda}{hc} \right) \Delta r Q_E T_O O_A \left[ \frac{A_T}{r^2} \right] \left[ \frac{1}{4\pi} (P_A(\pi, r) \beta_A(r) + P_M(\pi, r) \beta_M(r)) e^{-2 \int_0^r \beta_{ex}(r') dr'} \right] \right] + B_D + B_S$$

where the variables are defined as follows (dimensionality of the variable is given in parentheses):

$r$  is the distance to the scattering particle (m),

$E_T$  is the transmitted laser energy (J),

$\lambda$  is the laser wavelength (m),

$h$  is Planck's constant (J s),

$c$  is the speed of light (m/s),

$A_T$  is the telescope area (m<sup>2</sup>),

$\Delta r$  is the range bin length (m),

$Q_E$  is the detector quantum efficiency,

$T_O$  is the system optical efficiency,

$O_A(r)$  is the transmitter-receiver overlap function,

$P_A(\pi, r)$  is the aerosol backscatter phase function (sr<sup>-1</sup>),

$P_M(\pi, r)$  is the molecular backscatter phase function (sr<sup>-1</sup>),

$\beta_A(r)$  is the aerosol volume total scattering coefficient (m<sup>-1</sup>),

$\beta_M(r)$  is the molecular volume total scattering coefficient (m<sup>-1</sup>),

$\sigma(r)$  is the volume total extinction coefficient (m<sup>-1</sup>),

$B_D$  is background signal due to detector thermal noise, and

$B_S$  is background signal due to solar (i.e., non-laser) photons.

The lidar equation as given above is the simplest form and is correct for a single scattering atmosphere (e.g., effects of multiple scattering have been neglected). For more complicated measurements the equation is modified by inclusion of additional instrumental and/or physical parameters (which have been suppressed in the above equation). As an example, to describe Doppler lidar a term relating to the wavelength shift must be explicitly included. Also, implicit in the equation is an assumption that the range bin length,  $\Delta r$ , is much greater than the laser pulse length. A further important point is that the parameters  $\beta(r)$ ,  $P(\pi,r)$  and  $\sigma(r)$  are taken to be implicit functions of wavelength.

Variables in the above equation are grouped in a specific way to illustrate different contributions to the detected signal. The first grouping in brackets consists entirely of instrumental parameters. The term  $\lambda/hc$  converts the laser energy to number of photons (the lidar equation can also be written in terms of power transmitted and power returned rather than photons). The second set of brackets,  $A_T/r^2$ , describes the solid angle viewed by the receiver. Typical lidar observing geometry is shown in Figure 6, and Refs. 7 or 8 can be consulted for a derivation of the geometry and the lidar equation.

The third set of brackets specifies the atmospheric physics. The term  $P(\pi,r)*\beta(r)$  describes the scattering at the particle, from either molecules or aerosols. The phase function,  $P(\pi,r)$ , describes the distribution of scattered energy and is defined as the radiation per unit solid angle scattered in a particular direction divided by the average radiation scattered in all directions. In this derivation the phase functions are normalized to  $4\pi$ :

$$\frac{1}{4\pi} \iint P(\theta, \phi) \sin\theta \, d\theta \, d\phi = 1$$

$$\iint P(\theta, \phi) \sin \theta \, d\theta \, d\phi = 4\pi$$

Hence, the factor  $4\pi$  in the denominator of the lidar equation normalizes the scattering phase function over all angles. The volume total scattering coefficient,  $\beta(r)$ , expresses the total area of the incident wave front acted on by the particles in a unit volume. Note that the phase function and the volume total scattering coefficient are often shown combined into the volume angular backscatter coefficient,  $\beta(\pi, r) = (P(\pi, r)/4\pi) * \beta(r)$ .

Finally, the exponential term describes the effect of attenuation that occurs as the laser pulse propagates from the transmitter to the scattering particle and back to the receiver. Known as the Beer-Bouguer-Lambert law, the exponential term describes attenuation that occurs due to the intervening atmosphere. The volume total extinction coefficient,  $\sigma(r)$ , describes the ability of a volume of particles to remove flux from the incident light beam. The attenuation can be due to

$$e^{-2 \int_0^r S(r') \beta(r') \, dr'}$$

both scattering and absorption by both aerosols and molecules. In many cases it is acceptable to neglect absorption, in which case the volume total extinction coefficient reduces to  $\sigma(r) = \beta_A(r) + \beta_M(r)$ . If, however, measurements such as differential absorption (e.g., DIAL) are being considered then the attenuation term requires much more careful treatment.

Examination of the basic scattering lidar equation illustrates several important characteristics of lidar performance. First, the number of detected photons is directly dependent upon several instrumental parameters. Increasing the laser pulse energy, increasing the telescope size, or increasing the detector efficiency all lead to an increase in detected photons. However,

increasing the laser pulse energy may not always be practical due to limitations of the laser or eye safety considerations. Instead, most lidar systems operate by performing pulse accumulation, or shot averaging, whereby multiple laser pulses are summed to produce one measurement. Pulse averaging is useful to overcome, for example, the solar background signal that degrades a lidar measurement. In some cases it is beneficial to use lasers with high repetition rates but low pulse energy, which can be particularly useful in cases where photon-counting detection is used.(57)(58)

It is easily seen that there are two separate contributions to the detected backscattered signal: one from aerosols and one from molecules. Thus, in regions where aerosols are not present, the detected backscattered signal will be due only to Rayleigh scattering. Two other contributions to the total measured signal are detector thermal noise and solar background noise. Either can become large enough to overwhelm the backscattered signal and render a measurement useless. To reduce solar background interference filters are used or, for more stringent filtering requirements, narrower filters such as Fabry-Perot interferometers may be used in conjunction with the interference filter.

Examination of the lidar equation also highlights the difficulty encountered in inverting lidar data: the scattering lidar equation is underdetermined. The atmosphere contributes to the detected signal by providing scattering at the particle and by attenuating the signal as it travels from the transmitter to the particle and back to the receiver. The extinction is seen to depend on the backscatter coefficient but in an integral form. Solutions to the equation therefore always require an assumption or a priori information to attain a solution. The functional dependence on both the

aerosol total volume backscatter coefficient and the volume total extinction coefficient has long been a stumbling point for lidar researchers.

Several approaches have been used to solve the lidar equation, some more suitable than others. A simple approach is to use atmospheric models to calculate  $\sigma(r)$ . While simple, this method is unacceptable for quantitative studies of aerosol impact on climate. An improved method relies on having an independent measure of  $\beta_A(r)$  that can be used to solve the lidar equation at one altitude. Solutions at subsequent altitudes can then be obtained by differentiation of the profile.(59) This so-called slope method works well unless inhomogeneities, such as clouds or smoke plumes, are present. A less problematic approach is to start at high altitudes, where Rayleigh scattering dominates, and use backwards integration to solve for  $\beta_A(r)$  at successively lower altitudes.(60)(61). The now-common method for solving the lidar equation is to assume an aerosol extinction-to-backscatter ratio,  $S_A(r) = \sigma_A(r)/\beta_A(r)$ . The ratio can be taken as constant over altitude, or allowed to vary by altitude. Choice of  $S_A$  is highly dependent upon the atmosphere being measured (e.g., continental, marine, smoke, etc.) and is also wavelength dependent.(62)

## CONCLUSION

The proliferation of lidar systems since the 1970's is testimony to the utility of lidar remote sensing. However, lidar remote sensing is not without limitations. Lidar instruments are expensive, driven by the cost of lasers custom designed to meet specific measurement needs. Ground-based lidar systems do not provide useful measurements in rain or snow, and lidar

signals cannot penetrate dense clouds (an optical depth of about 5 is the maximum that can usually be penetrated). Eye safety is always a concern, both in the laboratory and for aircraft flying above (and for airborne lidars, eye safety for ground observers is a concern).

Limitations notwithstanding, lidar provides a powerful tool for atmospheric studies. The ability to remotely measure the atmospheric state from the comfort of a laboratory is a prime advantage for lidar. Measurement of particulate characteristics by lidar can be much less disruptive than in situ methods (e.g., sedimentation, filtration, or inertial impaction). The incident laser light does not change the chemical composition or physical characteristics of the particle, and the physics of light-particle interactions is well known. Lidar systems are inherently volume sampling instruments, capable of providing representative measurements in a turbulent atmosphere. The highly collimated beam and short pulse length available from most lasers means the lidar can sample a specific vertical increment of atmosphere. Of course, the ability to provide altitude profiles of atmospheric variables is the most significant advantage for lidar remote sensing.

The utility of lidar for measuring profiles of atmospheric state variables is well demonstrated. The number of ground-based and airborne lidar systems has been steadily increasing since the 1970s when lasers first became widely available. The variety of parameters measured with lidar continues to increase, and surely the potential for new lidar measurements is not yet exhausted. Soon, spaceborne lidar systems will allow global profiling of clouds and aerosols, with other spaceborne lidar measurements certain to follow.

## REFERENCES

1. Rao, P.K.; Holmes, S.J.; Anderson, R.K.; Winston, J.S.; Lehr, P.E. *Weather Satellites: Systems, Data, and Environmental Applications*; American Meteorological Society: Boston, 1990.
2. Fiocco, G.; Smullin, L.D. Detection of scattering layers in the upper atmosphere (60-140 km) by optical radar. *Nature* **1963**, *199* (490), 1275-1276.
3. Collis, R.T.H. Lidar: a new atmospheric probe. *Quarterly Journal of the Royal Meteorological Society* **1966**, *92* (392), 220-230.
4. Hamilton, P.M. The use of lidar in air pollution studies. *Air & Water Pollution International Journal* **1966**, *10*, 427-434.
5. von Zahn, U.; von Cossart, G.; Fiedler, J.; Fricke, K.H.; Nelke, G.; Baumgarten, G.; Rees, D.; Hauchecorne, A.; Adolfsen, K. The ALOMAR Rayleigh/Mie/Raman lidar: objectives, configuration, and performance. *Annales Geophysicae-Atmospheres Hydrospheres and Space Sciences* **2000**, *18* (7), 815-833.
6. McCartney, E.J. *Optics of the Atmosphere, Scattering by Molecules and Particles*; Wiley & Sons: New York, 1976.
7. Liou, K-N. *An Introduction to Atmospheric Radiation*; Academic Press: New York, 1980.
8. Measures, R.M. *Laser Remote Sensing: Fundamentals and Applications*; Wiley-Interscience Publications: New York, 1984.
9. Penndorf, R. Tables of the refractive index for standard air and the Rayleigh scattering coefficient for the spectral region between 0.2 and 20.0  $\mu\text{m}$  and their application to atmospheric optics. *Journal of the Optical Society of America* **1957**, *47* (2), 176-182.
10. Fiocco, G.; DeWolf, J.B. Frequency spectrum of laser echoes from atmospheric constituents and determination of the aerosol content of the air. *Journal of the Atmospheric Sciences* **1968**, *25* (3), 488-496.
11. Benedetti-Michelangeli, G.; Congedati, F.; Fiocco, G. Measurement of aerosol motion and wind velocity in the lower troposphere by Doppler optical radar. *Journal of the Atmospheric Sciences* **1972**, *29* (5), 906-910.
12. Platt, C.M.R.; Reynolds, D.W.; Abshire, N.L. Satellite and lidar observations of the albedo, emittance, and optical depth of cirrus compared to model calculations. *Monthly Weather Review* **1980**, *108* (2), 195-204.

13. Sassen, K.; Grund, C.J.; Spinhirne, J.D.; Hardesty, M.; Alvarez, J.M. The 27-28 October 1986 FIRE IFO cirrus case study: a five lidar overview of cloud structure and evolution. *Monthly Weather Review* **1990**, *118* (11), 2288-2311.
14. Spinhirne, J.D.; Hart, W.D. Cirrus structure and radiative parameters from airborne lidar and spectral radiometer observations: the 28 October 1986 FIRE study. *Monthly Weather Review* **1990**, *118* (11), 2329-2343.
15. Spinhirne, J.D.; Hart, W.D.; Hlavka, D.L. Cirrus infrared parameters and shortwave reflectance relations from observations. *Journal of the Atmospheric Sciences* **1996**, *53* (10), 1438-1458.
16. Collis, R.T.H. Lidar for routine meteorological observations. *Bulletin of the American Meteorological Society* **1969**, *50* (9), 688-694.
17. Reagan, J.; Apte, M.; Ben-David, A.; Herman, B. Assessment of aerosol extinction to backscatter ratio measurements made at 694.3 nm in Tucson, Arizona. *Aerosol Science & Technology* **1988**, *8* (3), 215-226.
18. Ansmann, A.; Riesbesell, M.; Weitkamp, C. Measurement of atmospheric extinction profiles with Raman lidar. *Optics Letters* **1990**, *15* (13), 746-748.
19. Welton, E.J.; Voss, K.J.; Gordon, H.R.; Maring, H.; Smirnov, A.; Holben, B.; Schmid, B.; Livingston, J.M.; Russell, P.B.; Durkee, P.A.; Formenti, P.; Andreae, M.O. Ground-based lidar measurements of aerosols during ACE-2: Instrument description, results, and comparisons with other ground-based and airborne measurements. *Tellus B* **2000**, *52* (2), 635-650.
20. Schotland, R.M.; Sassen, K.; Stone, R. Observations by lidar of linear depolarization ratios for hydrometeors. *Journal of Applied Meteorology* **1971**, *10*, 1011-1017.
21. Pal, S.R.; Carswell, A.I. Polarization properties of lidar backscattering from clouds. *Applied Optics* **1973**, *12* (7), 1530-1535.
22. Spinhirne, J.D.; Hansen, M.Z.; Simpson, J. The structure and phase of cloud tops as observed by polarization lidar. *Journal of Climate and Applied Meteorology* **1983**, *22* (8), 1319-1331.
23. Sassen, K. The polarization lidar technique for cloud research. *Bulletin of the American Meteorological Society* **1991**, *72* (12), 1848-1866.
24. Couch, R.H.; Rowland, C.W.; Ellis, K.S.; Blythe, M.P.; Regan, C.R.; Koch, M.R.; Antill, C.W.; Kitchen, W.L.; Cox, J.W.; DeLorme, J.F.; Crockett, S.K.; Remus, R.W.; Casas, J.C.; Hunt, W.H. Lidar In-space Technology Experiment (LITE): NASA's first in-space lidar system for atmospheric research. *Optical Engineering* **1991**, *30* (1), 88-95.

25. Zwally, H.J.; Schutz, B.; Abdalati, W.; Abshire, J.; Bentley, C.; Brenner, A.; Bufton, J.; Dezio, J.; Hancock, D.; Harding, D.; Herring, T.; Minster, B.; Quinn, K.; Palm, S.; Spinhirne, J.; Thomas, R. ICESat's laser measurements of polar ice, atmosphere, ocean, and land. *Journal of Geodynamics*, *in press*.
26. Winker, D.; Wielicki, B. The PICASSO-CENA mission. In *Sensors, Systems, and Next Generation Satellites*, Proceedings of SPIE vol. 3870, Florence, Italy, 20-23 September, 1999; Fujisada, H.; Lurie, J.B. Eds.; SPIE: Bellingham, 1999; 26-36.
27. Hall, F.F., Jr.; Huffaker, R.M.; Hardesty, R.M.; Jackson, T.E.; Lawrence, T.R.; Post, M.J.; Richter, R.A.; Weber, B.F. Wind measurement accuracy of the NOAA pulsed infrared Doppler lidar. *Applied Optics* **1984**, *23* (15), 2503-2506.
28. Huffaker, R.M.; Hardesty, R.M. Remote sensing of atmospheric wind velocities using solid-state and CO<sub>2</sub> coherent laser systems. *Proceedings of the IEEE* **1996**, *84* (2), 181-204.
29. Rothermal, J.; Cutten, D.R.; Hardesty, R.M.; Menzies, R.T.; Howell, J.N.; Johnson, S.C.; Tratt, D.M.; Olivier, L.D.; Banta, R.M. The Multi-center Airborne Coherent Atmospheric Wind Sensor. *Bulletin of the American Meteorological Society* **1998**, *79* (4), 581-599.
30. Rye, B.J. Comparative precision of distributed-backscatter Doppler lidars. *Applied Optics* **1995**, *34* (36), 8341-8344.
31. Bloom, S.H.; Kremer, R.; Searcy, P.A.; Rivers, M.; Menders, J.; Korevaar, E. Long-range, noncoherent laser Doppler velocimeter. *Optics Letters* **1991**, *16* (22), 1794-1796.
32. Abreu, V.J.; Barnes, J.E.; Hays, P.B. Observations of winds with an incoherent lidar detector. *Applied Optics* **1992**, *31* (22), 4509-4514.
33. Korb, C.L.; Gentry, B.M.; Li, S.X. Edge technique Doppler lidar wind measurements with high vertical resolution. *Applied Optics* **1997**, *36* (24), 5976-5983.
34. McGill, M.J.; Skinner, W.R.; Irgang, T.D. Validation of wind profiles measured with incoherent Doppler lidar. *Applied Optics* **1997**, *36* (9), 1928-1939.
35. Garnier, A.; Chanin, M.L. Description of a Doppler Rayleigh lidar for measuring winds in the middle atmosphere. *Applied Physics B* **1992**, *55* (1), 35-40.
36. Gentry, B.M.; Chen, H.; Li, S.X. Wind measurements with 355-nm molecular Doppler lidar. *Optics Letters* **2000**, *25* (17), 1231-1233.
37. Irgang, T.D.; Hays, P.B.; Skinner, W.R. Two-channel direct-detection Doppler lidar employing a charge-coupled device as a detector. *Applied Optics* **2002**, *41* (6), 1145-1155.
38. Melfi, S.H.; Lawrence, J.D., Jr.; McCormick, M.P. Observation of Raman scattering by water vapor in the atmosphere. *Applied Physics Letters* **1969**, *15* (9), 295-297.

39. Grant, W.B. Differential absorption and Raman lidar for water vapor profile measurements: a review. *Optical Engineering* **1991**, *30* (1), 40-48.
40. Lazzarotto, B.; Frioud, M.; Larcheveque, G.; Mitev, V.; Quaglia, P.; Simeonov, V.; Thompson, A.; van den Bergh, H.; Calpini, B. Ozone and water vapor measurements by Raman lidar in the planetary boundary layer: error sources and field measurements. *Applied Optics*, **2001**, *40* (18) 2985-2997.
41. Keckhut, P.; Chanin, M.L.; Hauchecorne, A. Stratosphere temperature measurement using Raman lidar. *Applied Optics* **1990**, *29* (34) 5182-5186.
42. Shibata, T.; Sakai, T.; Hayashi, M.; Ojio, T.; Kwon, S.A.; Iwasaka, Y. Raman lidar observations: simultaneous measurements of water vapor, temperature, and aerosol vertical profiles. *Journal of Geomagnetism and Geoelectricity* **1996**, *48* (9), 1127-1135.
43. Schwiesow, R.L. Lidar measurement of boundary layer variables. In *Probing the Atmospheric Boundary Layer*; Lenschow, D.H., Ed.; American Meteorological Society: Boston, 1986; 139-162.
44. Bills, R.E.; Gardner, C.S.; She, C-Y. Narrowband lidar technique for sodium temperature and Doppler wind observations of the upper atmosphere. *Optical Engineering* **1991**, *30* (1), 13-21.
45. Shipley, S.T.; Tracy, D.H.; Eloranta, E.W.; Trauger, J.T.; Sroga, J.T.; Roesler, F.L.; Weinman, J.A. A High spectral resolution lidar to measure optical scattering properties of atmospheric aerosols, part I: instrumentation and theory. *Applied Optics* **1983**, *22* (23), 3716-3724.
46. Grund, C.J.; Eloranta, E.W. University of Wisconsin high spectral resolution lidar. *Optical Engineering* **1991**, *30* (1), 6-12.
47. Browell, E.V.; Wilkerson, T.D.; McIlrath, T.J. Water vapor differential absorption lidar development and evaluation. *Applied Optics* **1979**, *18* (20), 3474-3483.
48. McDermid, I.S.; Haner, D.A.; Kleiman, M.M.; Walsh, T.D.; White, M.L. Differential absorption lidar systems for tropospheric and stratospheric ozone measurements. *Optical Engineering* **1991**, *30* (1), 22-30.
49. Browell, E.V.; Gregory, G.L.; Harriss, R.C.; Kirchoff, V.W.J.H. Tropospheric ozone and aerosol distributions across the Amazon basin. *Journal of Geophysical Research - Atmospheres* **1988**, *93* (D2), 1431-1451.
50. Bufton, J.L.; Garvin, J.B.; Cavanaugh, J.F.; Ramos-Izquierdo, R.; Clem, T.D.; Krabill, W.B. Airborne lidar for profiling of surface topography. *Optical Engineering* **1991**, *30* (1), 72-78.

51. Blair, J.B.; Rabine, D.L.; Hofton, M.A. The Laser Vegetation Imaging Sensor: a medium-altitude, digitisation-only, airborne laser altimeter for mapping vegetation and topography. *ISPRS Journal of Photogrammetry and Remote Sensing* **1999**, *54* (2-3), 115-122.
52. Krabill, W.; Thomas, R.; Jezek, K.; Kuivinen, K.; Manizade, S. Greenland ice-sheet thickness measured by laser altimetry. *Geophysical Research Letters* **1995**, *22* (17), 2341-2344.
53. Garvin, J.B.; Sakimoto, S.E.H.; Frawley, J.J.; Schnetzler, C. North polar region craterforms on Mars: geometric characteristics from the Mars Orbiter Laser Altimeter. *ICARUS* **2000**, *144* (2), 329-352.
54. Hoge, F.E.; Swift, R.N. Airborne simultaneous spectroscopic detection of laser induced water Raman backscatter and fluorescence from chlorophyll-a and other naturally occurring pigments. *Applied Optics* **1981**, *20* (18), 3197-3205.
55. Chekalyuk, A.M.; Hoge, F.E.; Wright, C.W.; Swift, R.N.; Yungel, J.K. Airborne test of laser pump-and-probe technique for assessment of phytoplankton photochemical characteristics. *Photosynthesis Research* **2000**, *66* (1-2), 45-56.
56. Hwang, P.A.; Krabill, W.B.; Wright, W.; Swift, R.N.; Walsh, E.J. Airborne scanning lidar measurement of ocean waves. *Remote Sensing of Environment* **2000**, *73* (2), 236-246.
57. Campbell, J.R.; Hlavka, D.L.; Welton, E.J.; Flynn, C.J.; Turner, D.D.; Spinhirne, J.D.; Scott, V.S.; Hwang, I.H. Full-time, eye-safe cloud and aerosol lidar observation at Atmospheric Radiation Measurement Program sites: instrument and data processing. *Journal of Atmospheric and Oceanic Technology*, *in press*.
58. McGill, M.J.; Hlavka, D.L.; Hart, W.D.; Scott, V.S.; Spinhirne, J.D.; Schmid, B. The Cloud Physics Lidar: instrument design and initial measurement results. *Applied Optics*, *in press*.
59. Collis, R.T.H.; Russell, P.B. Lidar measurement of particles and gases by elastic backscattering and differential absorption. In *Laser Monitoring of the Atmosphere*, Hinkley, E.D., Ed.; Springer-Verlag: New York, 1976.
60. Klett, J.D. Stable analytical inversion solution for processing lidar returns. *Applied Optics* **1981**, *20* (2), 211-220.
61. Klett, J.D. Lidar inversions with variable backscatter/extinction ratios. *Applied Optics* **1985**, *24* (11), 1638-1643.
62. Ackerman, J. The extinction-to-backscatter ratio of tropospheric aerosol: a numerical study. *Journal of Atmospheric and Oceanic Technology* **1998**, *15*, 1043-1050.

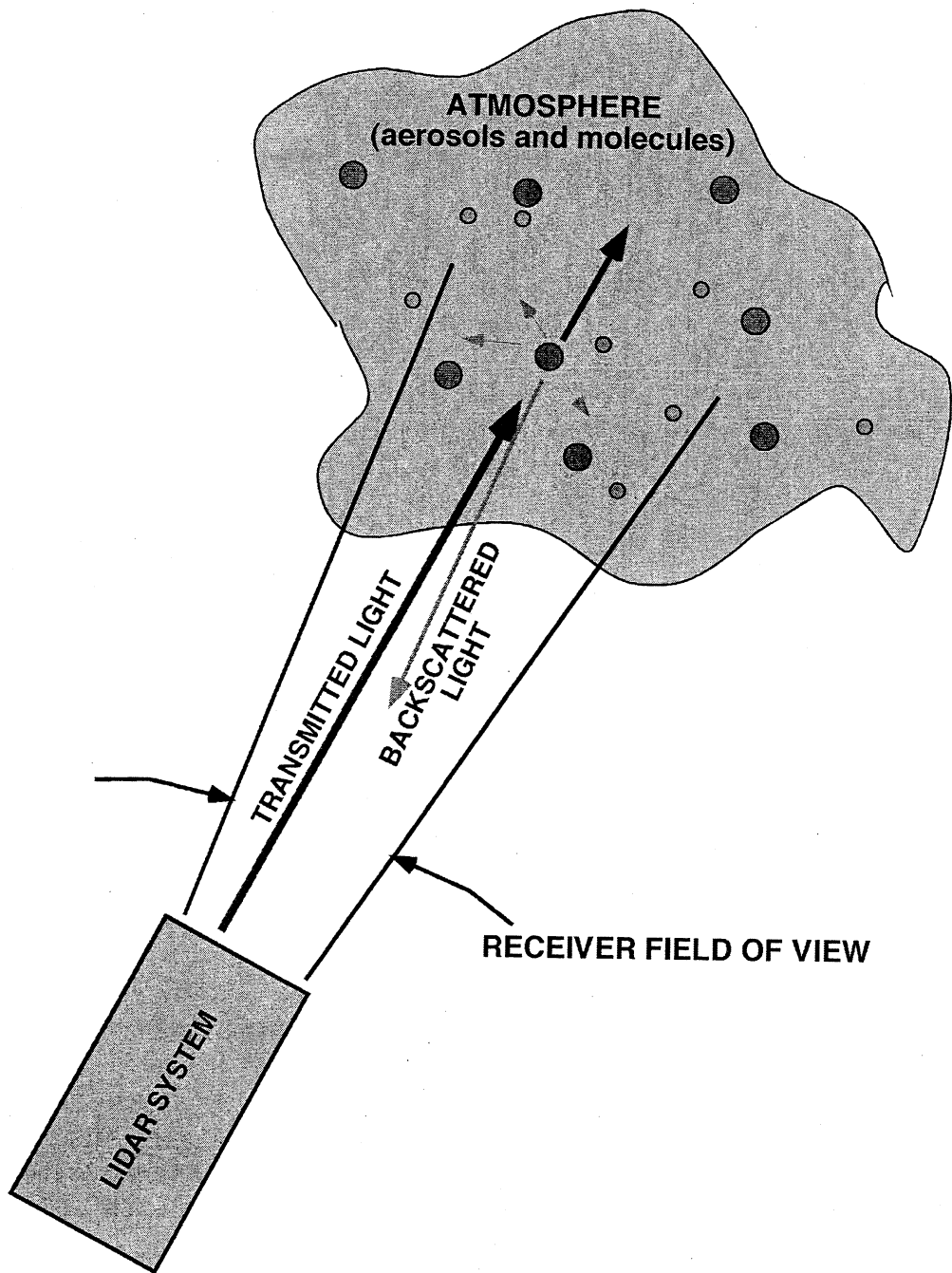
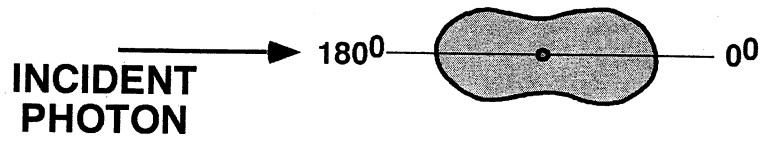


Figure 1: Basic concept of lidar remote sensing. The lidar system transmits laser light to the atmosphere where it is scattered by aerosols and molecules. Some fraction of the scattered light finds its way back to the receiving telescope where a receiver and detector(s) can analyze the information content of the signal.

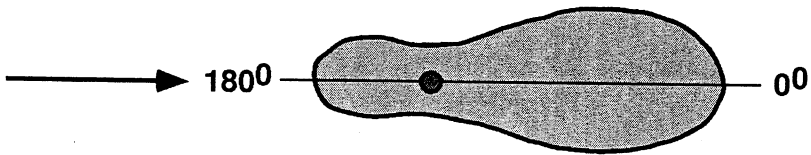


a)



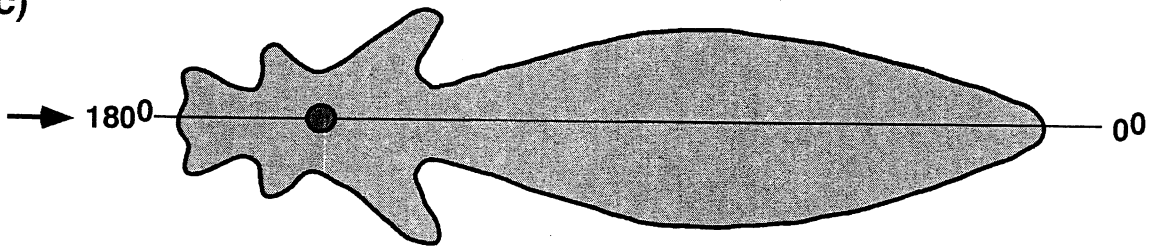
**SMALL PARTICLES  
(RAYLEIGH SCATTERING)**  
 $r < 0.03 \lambda$

b)



**LARGE PARTICLES**  
 $r = 0.25 \lambda$

c)



**LARGER PARTICLES  
(MIE SCATTERING)**  
 $r \gg \lambda$

Figure 2: Scattering phase functions describe the pattern of energy scattered by particles. Larger particles generate more complex scattering patterns.



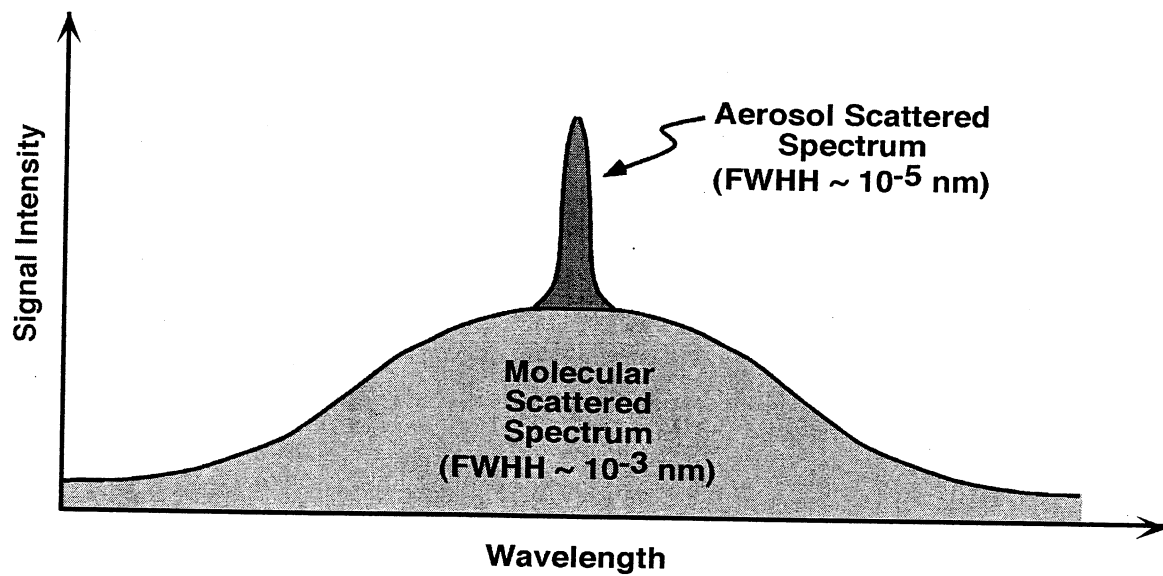


Figure 3: Spectral signatures of aerosol and molecular scattering. The molecular scattered signal is Doppler-broadened due to random thermal motions. Aerosols, in contrast, are heavier and have little thermal motion, thus the aerosol scattered signal is not appreciably broadened.



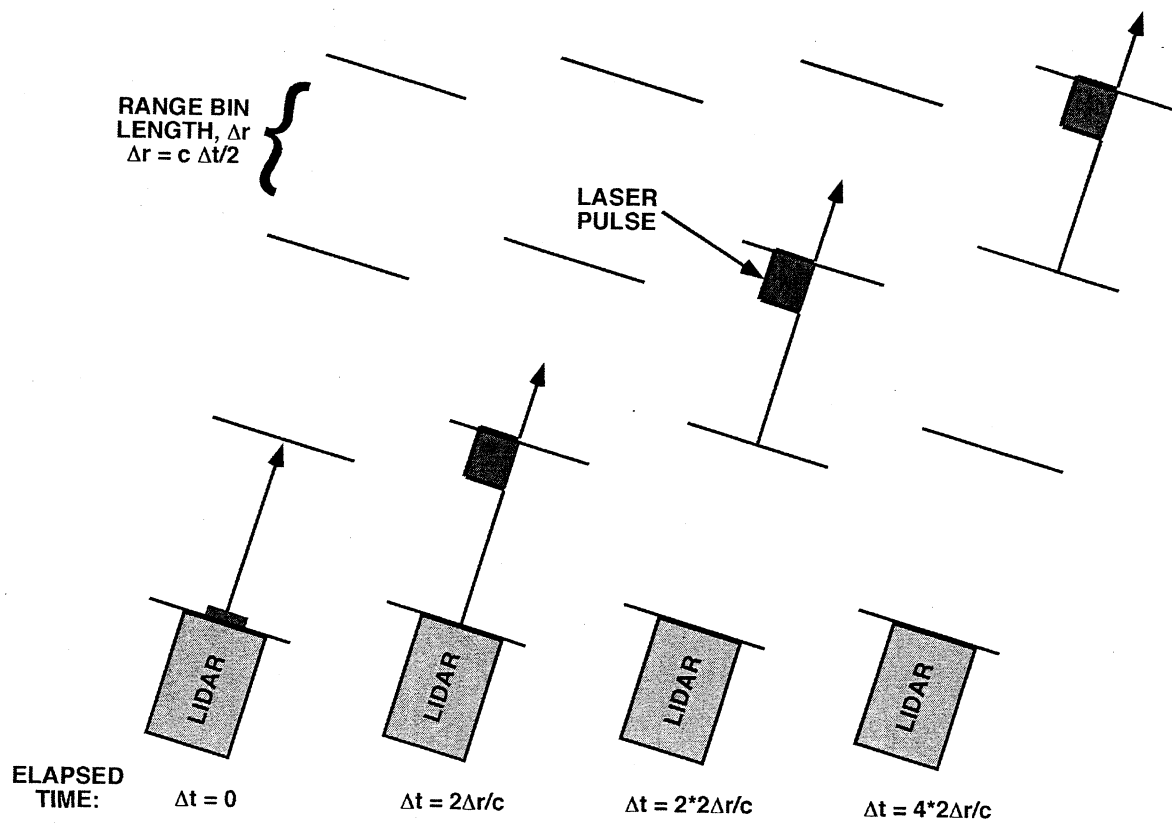


Figure 4: Pulsed lasers allow range resolution of the atmosphere. Because laser radiation propagates through the atmosphere at the speed of light, return signal can be measured in discrete path length elements. In this way the atmospheric state at each altitude increment can be independently measured.



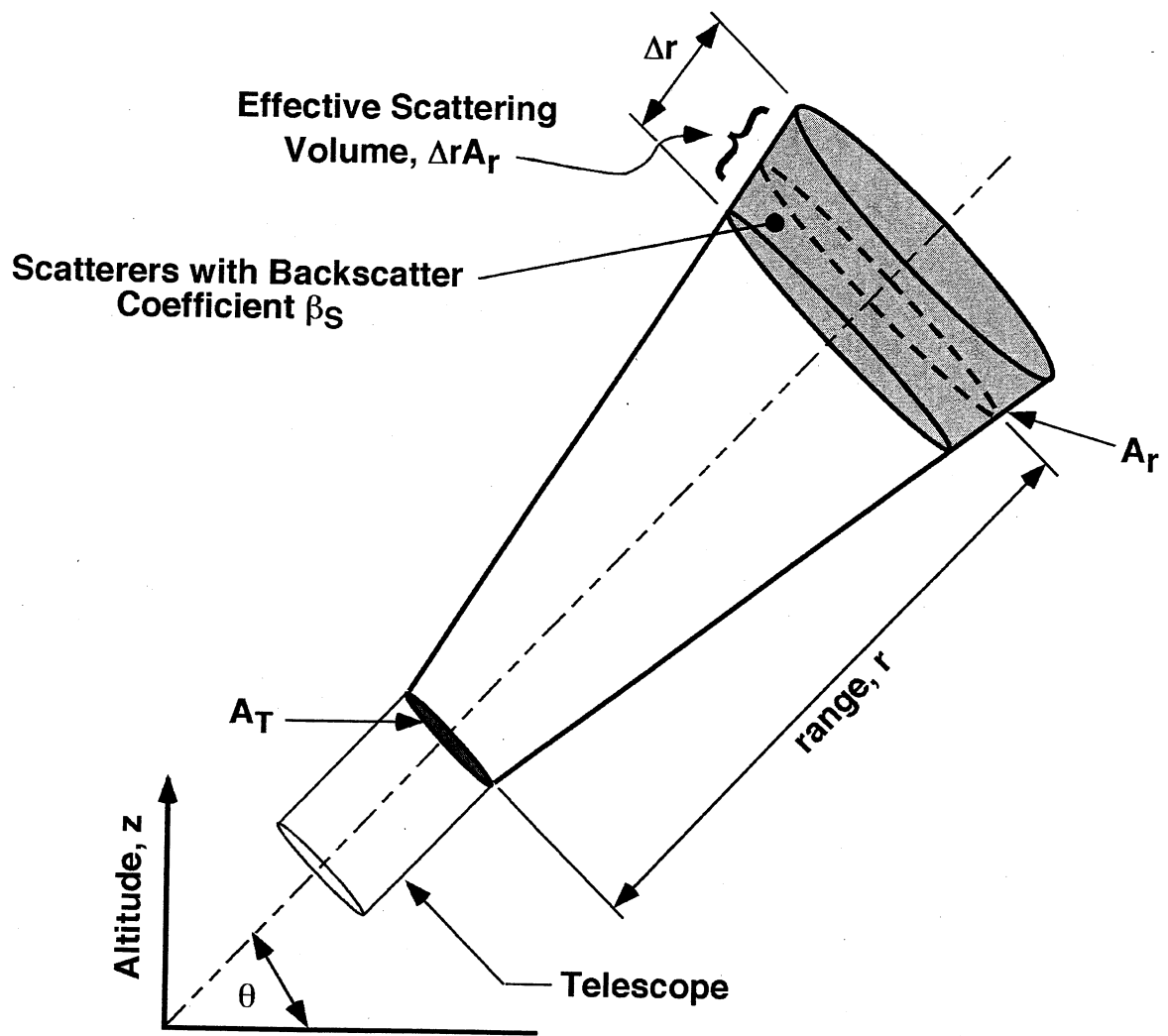


Figure 5: Lidar observing geometry.  $\Delta r$  is the range bin length,  $A_T$  is the telescope area, and  $A_r$  is the cross-sectional area of the laser beam at range  $r$ .



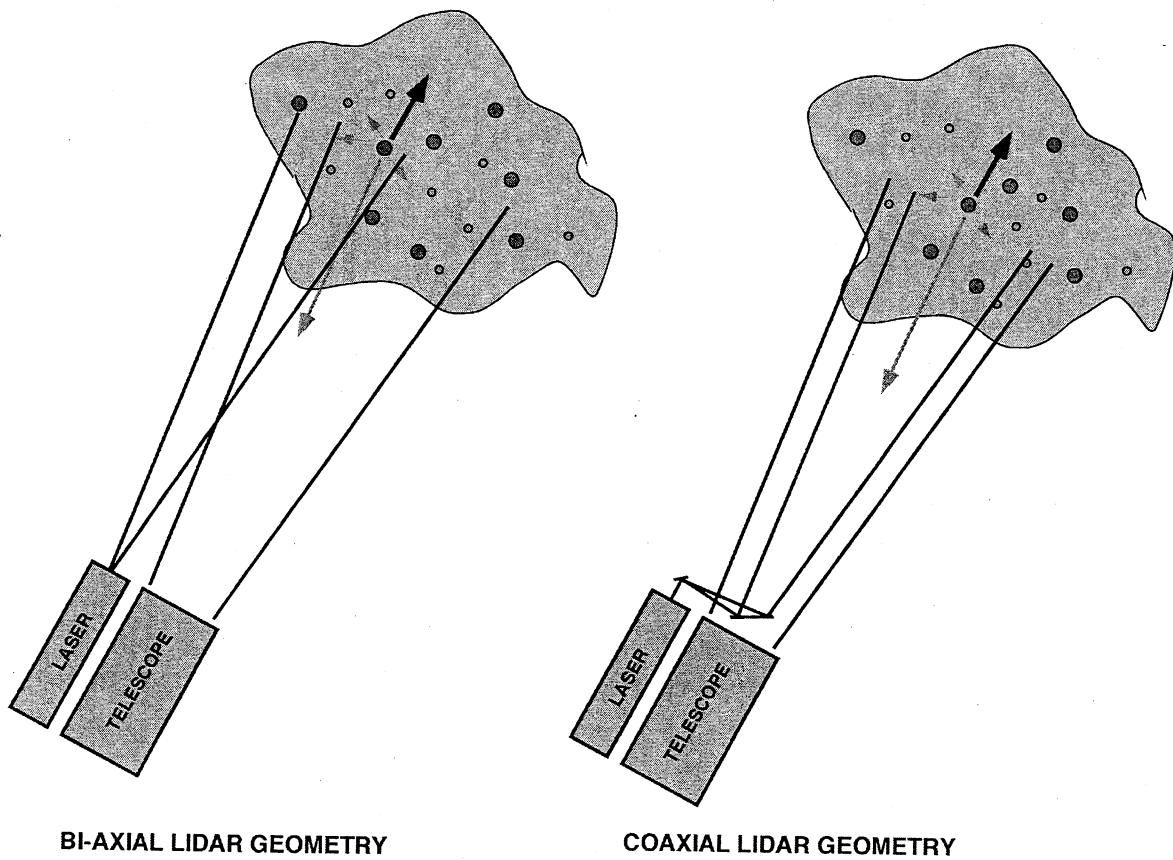


Figure 6: Lidar viewing geometry for bi-axial and coaxial systems. Note that the coaxial system attains full overlap at lower altitude than the biaxial system.

